Cooperative up-conversion in Eu^{3+},Yb^{3+}-doped SiO_2–PbO–PbF_2–CdF_2 oxyfluoride glass

CrossMark

P.A. Loiko [a], G.E. Rachkovskaya [b], G.B. Zakharevich [b], A.A. Kornienko [c], E.B. Dunina [c], A.S. Yasukevich [a], K.V. Yumashev [a],*

[a] Center for Optical Materials and Technologies, Belarusian National Technical University, 220013, Belarus, Minsk, 65/17 Nezavisimosti Ave.
[b] Glass and Ceramics Technology Department, Belarusian State Technological University, 220006, Belarus, Minsk, 13a Sverdlova St.
[c] Vitebsk State Technological University, 210035, Belarus, Vitebsk, 72 Moskovskaya Ave.

ABSTRACT

Novel oxyfluoride glass doped with YbF_3 and Eu_2O_3 is synthesized in the SiO_2–PbO–PbF_2–CdF_2 system by melt-quenching technique. Its physical properties, as well as the optical absorption of Eu^{3+} and Yb^{3+} ions are studied. Spectroscopic properties of Eu^{3+} ions are modeled within modified Judd–Ofelt theory, yielding absorption oscillator strength, luminescence branching ratios and radiative lifetime of $^5D_0$ state. Intrinsic emission of Eu^{3+} ions under direct excitation in the UV, as well as up-conversion luminescence under near-IR excitation via cooperative energy transfer, $2Yb^{3+} \rightarrow Eu^{3+}$, are studied. In the latter case, the glass provides intense reddish-orange emission with CIE coordinates $x = 0.636$, $y = 0.363$. The asymmetry parameter R for Eu^{3+} emission in the studied glass is about 8. The efficiency of this transfer mechanism is estimated from shortening of $^2F_{5/2}(Yb^{3+})$ lifetime to be $10 \pm 1\%$.

1. Introduction

Oxyfluoride glasses and nanophase glass-ceramics nowadays attract attention as proper hosts for efficient up-conversion in the Yb^{3+}–RE^{3+} system, where RE^{3+} is trivalent rare-earth ions like Er [1,2] (investigated in pioneering work of F. Auzel et al. [3]), Tm, and Ho [4–6]. They combine good spectroscopic properties of fluoride materials related with low phonon energies, as well as chemical stability, good thermal and mechanical properties of oxide compounds [7,8]. Thus, one can obtain intense and multicolor visible emissions [9,10] under near-IR excitation by commercial InGaAs laser diodes. Such glasses can be easily synthesized by standard melt-quenching technique (with beneficial low melting point); and can be used for the production of transparent glass-ceramics containing rare-earth-doped fluoride nanocrystals like MF_2, LnF_3 or $NaLnF_4$ [11–15] with enhanced luminescent properties.

Trivalent europium ions, Eu^{3+}, doped into various solid-state hosts (thin films, polymers, nanopowders, glasses, glass-ceramics or single crystals) attract attention due to their intense red emission near ~612 nm related with $^5D_0 \rightarrow {}^7F_2$ transition within $4f^6$ electronic shell [16,17]. Such materials have commercially-recognized applications in tricolor lamps, field emission displays, cathode-ray tubes and solid-state lightning.

The system Yb^{3+}–Eu^{3+} can also provide red emission via so-called cooperative energy transfer from excited Yb^{3+} ion pair to single Eu^{3+} ion [18]. Unfortunately, limited number of papers devoted to such process has been published to the moment [18–26]. Detailed spectroscopic investigation of Eu,Yb-doped oxyfluoroborate H_3BO_3–BaF_2 glass is presented in [18]. However, the efficiency of ET was not determined, and red up-conversion luminescence was partially suppressed by cooperative emission of Yb^{3+} pairs. In [20], sol–gel silica glass was studied, showing high impact of parasitic Tm^{3+} emission. The authors of [19] highlighted the role of erbium in triply-doped Yb:Er:Eu tellurite TeO_2–BaF_2 glass. Yb, Eu-codoped Y_2O_3 [21,26], $Y_3Al_5O_{12}$, $Gd_3Ga_5O_{12}$ [23] and BaB_4O_7 [25] nano-powders were studied, while [24] present results on Eu:$KYb(WO_4)_2$ single crystal. Thus, detailed spectroscopic investigation for oxyfluoride glasses is still relevant.

In the present paper, we report on synthesis, investigation of basic physical properties, as well as optical absorption and luminescence of novel SiO_2–PbO–PbF_2–CdF_2 oxyfluoride glass doped with YbF_3 and Eu_2O_3, accompanied with theoretical determination of basic spectroscopic properties with modified Judd–Ofelt theory. The potential of this glass for production of glass-ceramic orange-red phosphor is also analyzed.

2. Glass synthesis and thermal studies

The studied oxyfluoride glass was synthesized by melt-quenching technique in the system $40SiO_2$–$20PbO$–$30PbF_2$–$10CdF_2$ (the composition is in mol%); it was doped with YbF_3 (1.0 mol%) and Eu_2O_3

* Corresponding author at: 220013 Belarus, Minsk, 65/17 Nezavisimosti Ave., Center for Optical Materials and Technologies, Belarusian National Technical University. Tel.: +375 17 293 91 88; fax: +375 17 292 62 86.
E-mail address: k.yumashev@tut.by (K.V. Yumashev).

(1.0 mol%). The raw materials (99.9%-purity) were weighted and homogenized in 25 cm^3 corundum crucible. The synthesis was performed at ~900 ± 50 °C in the electric furnace in air. The duration of synthesis at maximum temperature was 0.5 h. The melt was then cast to the steel surface and annealed at ~300 °C for 2 h in the muffle furnace. Then the glass boule was cooled down to room temperature. It was transparent with slight yellow coloration and do not contain cracks, signs of opalescence and air bubbles. X-ray diffraction confirmed amorphous nature of as-cast glass. The glass density ρ was measured by hydrostatic method, $\rho = 5.26 \pm 0.01$ g/cm^3, so the concentration of active ions N_{Eu} is 2.4 (Eu^{3+}) and 1.2 ± 0.2 (Yb^{3+}) × 10^{20} cm^{-3}.

Differential scanning calorimetry, DSC, curve for studied glass was determined with a Netzch DSC 404F3 Pegasus instrument, see Fig. 1(a). The glass transition temperature T_g is 385 °C. At the temperature of $T_p =$ 508 °C, the first crystallization peak is observed. It is attributed to the precipitation of cubic (Pb,Cd)F$_2$ solid-solution, as determined from XRD studies, see Fig. 1(b) with the XRD spectrum of corresponding glass-ceramic sample. Particularly, the shift of the observed diffraction peaks to higher 2θ values, as compared with bulk PbF$_2$ crystal (that mean the decrease of lattice parameter a) indicates that Cd partially replaces Pb in the PbF$_2$ structure, as ionic radius of Cd^{2+} is substantially lower than that of Pb^{2+}. The difference $\Delta = T_p - T_g$ that is called glass thermal stability factor, is then equal to 123 °C. Such a large value indicate that studied glass has good potential for synthesis of nanophase glass-ceramics containing Eu,Yb-codoped (Pb,Cd)F$_2$ nanocrystals. Thermal expansion was measured with horizontal dilatometer, Netzsch 402 PC, $\alpha = 10.3 \pm 0.2 \times 10^{-6}$ K^{-1}.

Basic physical properties of studied glass are summarized in Table 1.

3. Optical absorption

Firstly, refractive index of the studied glass, $n = 1.60 \pm 0.01$, was measured at the wavelength of 650 nm by immersion method. Optical
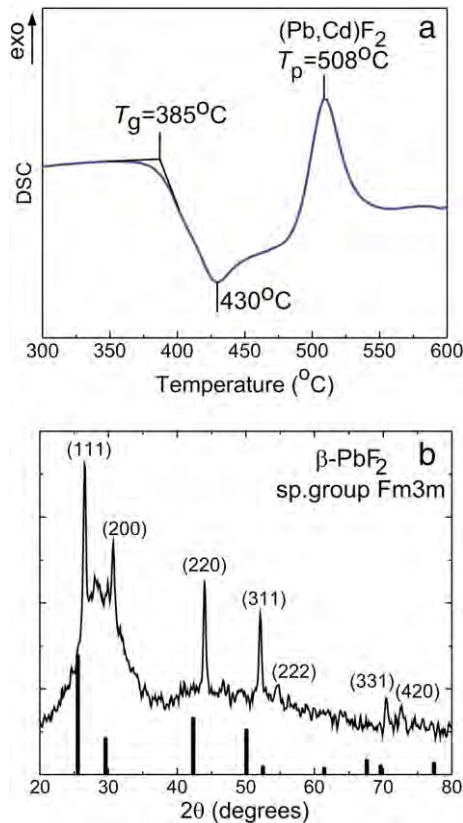

Fig. 1. Differential scanning calorimetry (DSC) curve for Eu,Yb-doped oxyfluoride glass: T_g is the glass transition temperature, T_p is the peak crystallization temperature for (Pb,Cd)F$_2$ phase (a), XRD spectrum of glass-ceramics heat-treated at 420 °C (b).

Table 1
Physical properties of Eu,Yb-doped SiO$_2$–PbO–PbF$_2$–CdF$_2$ glass.

Property	Value
Melting point	900 ± 50 °C
Glass transition temperature, T_g	385 °C
Crystallization temperature, T_p	508 °C, (Pb, Cd)F$_2$ phase
Density, ρ	5.26 g/cm^3
Thermal expansion, α	10.3×10^{-6} K^{-1}
Refractive index, n	1.60 at 650 nm
Bandgap, E_g	3.42 ± 0.05 eV
Content of dopants	Eu$_2$O$_3$,YbF$_3$ (1.0 mol%)
Eu^{3+} concentration, N_{Eu}	2.4×10^{20} cm^{-3}
Yb^{3+} concentration, N_{Yb}	1.2×10^{20} cm^{-3}
Absorption coefficient, α_{abs}	0.8 cm^{-1} (Yb^{3+}, at 960 nm)
	2.2 cm^{-1} (Eu^{3+}, at 400 nm)

absorption was studied by a Varian Cary-5000 instrument (in the range 0.3–2.8 μm, spectral bandwidth, SBW, was 0.5 nm). For this, 2-mm thick polished plate was used.

Optical absorption spectrum of the studied glass contains characteristic bands of Eu^{3+} and Yb^{3+} ions, see Fig. 2. In Table 2, the position of observed absorption bands of Eu^{3+} (both in nm and cm^{-1}) is listed. Bands in the visible are related with transitions from ground $^7F_0$ and lower-lying excited $^7F_1$ states (the latter is separated by 300 cm^{-1} gap and hence it is thermally- populated) of Eu^{3+} to a higher-lying ^5D_J ($J = 0, 1, 2, 3$) and $^5L_6$ excited states. Bands in the near-IR are related with $^2F_{7/2} \rightarrow {}^2F_{5/2}$ transition for Yb^{3+} (around 1 μm) and $^7F_{0,1} \rightarrow {}^7F_6$ transitions for Eu^{3+} (spanning across 1.8–2.4 μm). After 2.8 μm, the absorption of OH-groups was detected. The inset in Fig. 2 shows so-called Tauc plot. From this plot, electronic bandgap E_g for studied glass is determined to be 3.42 ± 0.05 eV (the position of UV absorption edge is 362 ± 5 nm). The most intense transition in the visible is the $^7F_0 \rightarrow {}^5L_6$ one. It is positioned at 393 nm and correspond to peak absorption coefficient, $\alpha = 2.2$ cm^{-1}. Thus, it is suitable for the excitation of intrinsic Eu^{3+} emission by InGaN laser diode emitting around 0.4 μm. The value of α coefficient for the radiation of InGaAs diodes emitting at 960 nm, is 0.8 cm^{-1}.

4. Judd–Ofelt modeling

The absorption oscillator strengths, f_{exp}, for observed absorption bands of Eu^{3+} in the studied glass were calculated from measured absorption spectra $\alpha(\lambda)$:

$$f_{exp}(JJ') = \frac{m_e c^2}{\pi e^2 N_{Eu} \overline{\lambda}^2} \int \alpha(\lambda) d\lambda, \qquad (1)$$

where m_e and e are the electron mass and charge, c is the speed of light, $\overline{\lambda}$ is the coordinate of "center of gravity" of selected absorption band (mean wavelength), N_{Eu} is the concentration of Eu^{3+} ions, and the integration is performed over the selected absorption band related with J–J′ transition, see Table 2. The error for f_{exp} values is about 10%; it is mainly related with the uncertainty in the determination of N_{Eu} that was calculated from the initial batch composition.

The values of f were also modeled with conventional Judd–Ofelt (J–O) theory [27,28], as well as its modification for systems with strong configuration interaction (SCI) [29]. The oscillator strengths for J–J′ electric-dipole transitions are determined from the line strengths as:

$$f(JJ') = \frac{8\pi^2 m_e c \overline{\nu}}{3(2J+1)he^2} \frac{(n^2+2)^2}{9n} S_{ED}(JJ'), \qquad (2)$$

where n is the refractive index of the material and $\overline{\nu}$ is the mean wavenumber of selected transition. The line strengths of electric-dipole (ED) transitions depend substantially on the local field for
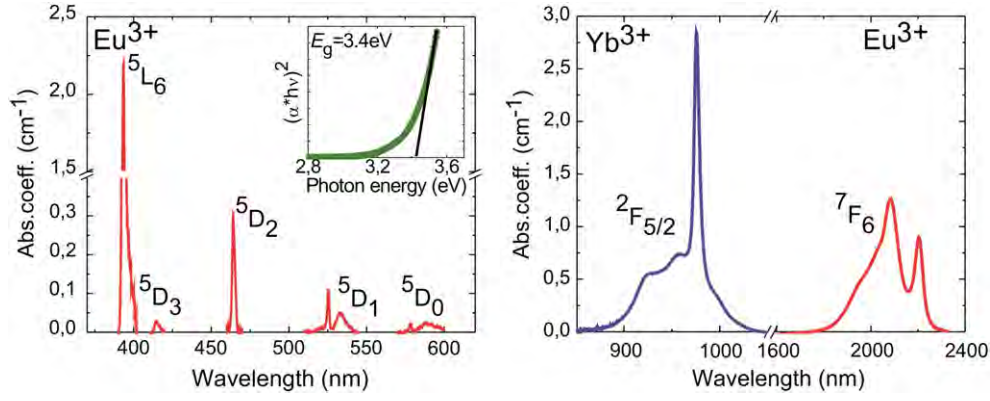
Fig. 2. Optical absorption of Eu,Yb-doped oxyfluoride glass in the visible (*left* graph, background losses are subtracted) and near-IR (*right* graph); *inset* represents Tauc plot.

considered ion embedded in the host material. Thus, their calculation is in accordance with the expression

$$S_{ED}(JJ') = \sum_{MM'} \left| \langle \gamma JM | \vec{D} | \gamma' J' M' \rangle \right|^2 \quad (3)$$

can lead to significant variation of the results in dependence on the model applied. This problem can be solved within perturbation theory:

$$\langle \gamma JM | = \langle \gamma [LS] JM | - \sum_{\psi} \frac{\langle \gamma [LS] JM | \hat{V} | \psi \rangle \langle \psi |}{E_{\gamma J} - E_{\psi}}, \quad (4a)$$

$$|\gamma' J' M' \rangle = |\gamma' [L'S'] J' M' \rangle + \sum_{\psi} \frac{|\psi \rangle \langle \psi | \hat{V} | \gamma' [L'S'] J' M' \rangle}{E_{\gamma' J'} - E_{\psi}}. \quad (4b)$$

Here ψ corresponds to the configurations of opposite parity like $4f^{N-1}5d$ and configuration with charge transfer, $\hat{V}$ is the perturbation operator. As a result, the matrix element of electric-dipole transition can be determined as:

$$\langle \gamma JM | \vec{D} | \gamma' J' M' \rangle = \sum_{\psi} \frac{\Delta_{\psi}}{E_{\gamma' J'} - \Delta_{\psi}} \frac{\langle \gamma [LS] JM | \vec{D} | \psi \rangle \langle \psi | \hat{V} | \gamma' [L'S'] J' M' \rangle}{\Delta_{\psi}} +$$
$$+ \sum_{\psi} \frac{\Delta_{\psi}}{E_{\gamma J} - \Delta_{\psi}} \frac{\langle \gamma [LS] JM | \hat{V} | \psi \rangle \langle \psi | \vec{D} | \gamma' [L'S'] J' M' \rangle}{\Delta_{\psi}}, \quad (5)$$

where Δ_{ψ} is the energy of excited configuration, $E_{\gamma J}$ and $E_{\gamma J'}$ are the multiplet energies.

On the basis of this expression, one can obtain formulas for line strengths under different assumptions about configuration interaction.

For instance, if we consider $E_{\gamma J} - \Delta_{\psi} \approx E_{\gamma J'} - \Delta_{\psi} \approx - \Delta_{\psi}$ (weak configuration interaction), it will be the case of J–O theory with

$$S_{ED}(JJ') = e^2 \sum_{k=2,4,6} \Omega_k \left\langle \gamma J \| U^k \| \gamma' J' \right\rangle^2. \quad (6)$$

The results obtained with this theory are presented in Table 2. The required reduced matrix elements $<\gamma J\|U^k\|\gamma'J'>$ were calculated by us on the wave functions of Eu^{3+} ion under the assumption of free-ion. The set of Judd–Ofelt parameters for studied glass is $\Omega_2 = 9.6$, $\Omega_4 = 16.5$ and $\Omega_6 = 3.1$ [10^{-20} cm^2].

More adequate description of obtained experimental oscillator strengths can be performed within so-called strong configuration interaction (SCI), Table 2. Indeed, in the latter case, root-mean-square (rms) deviation between f_{exp} and f_{WCI} values is lower, namely 0.06 (compare with 0.62 for J–O theory). The SCI approximation corresponds to equal energies of all excited configurations, $\Delta_{\psi} \approx \Delta$, so:

$$S_{ED}(JJ') = \frac{e^2}{4} \sum_{k=2,4,6} \Omega_k \left(\frac{\Delta}{\Delta - E_J} + \frac{\Delta}{\Delta - E_{J'}} \right)^2 \left\langle \gamma J \| U^k \| \gamma' J' \right\rangle^2. \quad (7)$$

For SCI theory, the set of modeling parameters is {$\Omega_2 = 6.7$, $\Omega_4 = 10.4$, $\Omega_6 = 2.7$ [10^{-10} cm^2] and $\Delta = 73140$ [cm^{-1}]}.

Both J–O theory and SCI approximations allow for the calculation of line strengths for ED transitions. The contribution of magnetic-dipole (MD) transitions with J–J' = 0, ±1 was calculated separately within the Russell–Saunders approximation on wave functions of Eu^{3+} ion under the assumption of free-ion.

More profound discussion about the use of WCI theory for special cases of Pr^{3+} and Eu^{3+} ions can be found in [30–32].
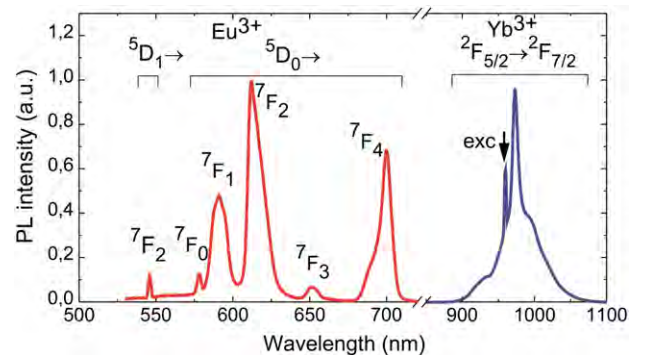
Table 2
Characterization of absorption bands of Eu^{3+} ions in Eu,Yb-doped oxyfluoride glass.

Transition	ν, cm^{-1}	λ, nm	$f_{exp} \times 10^6$	$f_{SCI} \times 10^6$	$f_{J-O} \times 10^6$
$^7F_{0,1} \rightarrow {}^7F_6$	4357	2204	5.74	5.77	6.23
	4800	2083			
$^7F_1 \rightarrow {}^5D_0$	17,301	578	0.08	0.04	0.04
$^7F_{0,1} \rightarrow {}^5D_1$	18,761	533	0.28	0.26	0.27
	19,047	525			
$^7F_0 \rightarrow {}^5D_2$	21,550	464	0.27	0.26	0.26
$^7F_1 \rightarrow {}^5D_3$	24,096	415	0.31	0.31	0.31
$^7F_0 \rightarrow {}^5L_6$	25,445	393	2.65	2.66	1.92
RMS dev.				0.06	0.62

Fig. 3. Intrinsic emissions of Eu^{3+} and Yb^{3+} ions for Eu,Yb-doped oxyfluoride glass (λ_{exc} = 401 and 960 nm, accordingly).

5. Photoluminescence

Intrinsic emissions of Eu^{3+} ions excited at ~0.4 μm (to $^5L_6$ state) are shown in Fig. 3. They were registered with lock-in amplifier and mono-chromator with a sensitive Hamamatsu C5460-01 detector. The spectrum contains bands centered at 578, 591, 612, 652 and 700 nm that are related with radiative transitions from metastable $^5D_0$ state to ^7F_J ones (J = 0, 1, 2, 3 and 4, accordingly). Moreover, a weak band around 545 nm is also detected (like in the previous papers [23–25], we attribute this band to $^5D_1 \rightarrow {}^7F_2$ transition of Eu^{3+}). Table 3 summarizes the position of observed emissions (both in nm and cm^{-1}). An important comment is that no blue emission around 450 nm (that is the indicator of $Eu^{3+} \rightarrow Eu^{2+}$ reduction) was observed. Intrinsic emission of Yb^{3+} excited at ~0.96 μm and spanning across 0.9–1.1 μm (related with $^2F_{5/2} \rightarrow {}^2F_{7/2}$ transition) is also shown in Fig. 3.

Eu^{3+} is known for its hyper-sensitive electric-dipole transition $^5D_0 \rightarrow {}^7F_2$ that is the indicator of symmetry of the ion site [33]. If the site has no inversion center, this transition will be dominant over $^5D_0 \rightarrow {}^7F_1$ magnetic-dipole one. In our case of amorphous as-cast glass, particularly this case is observed. Indeed, the relation of integrated intensities of above mentioned bands, defined as asymmetry parameter R, equals to 8:

$$R = \frac{I_{ED}\left({}^5D_0 \rightarrow {}^7F_2\right)}{I_{MD}\left({}^5D_0 \rightarrow {}^7F_1\right)}. \tag{8}$$

Determination of J–O parameters allows us to determine the luminescence branching ratios β for $^5D_0$ state. Both ED and MD transitions from $^5D_0$ to $^7F_0$ state are forbidden in accordance with the Wigner–Eckart theorem (as J = J' = 0). The observation of this transition in the PL spectrum (Fig. 3) can be due to the effect of J–J-mixing in the local field that cannot be taken into account for the utilized theories. For $^5D_0 \rightarrow {}^7F_1$ transition, the values of total angular momentum quantum numbers are J = 0 and J' = 1. In accordance with the Wigner–Eckart theorem, the possible k indices defining intensity parameters Ω_k, satisfy the relation $|J-J'| \leq k \leq J + J'$. Another words, $k = 1$, so oscillator strength for ED transition is defined solely by Ω_1 parameter that is zero in J–O theory (as well as WCI one). Thus, the value of $S_{ED}({}^5D_0 \rightarrow {}^7F_1)$ is zero in the J–O theory (pure MD transition). The value of $S_{MD}({}^5D_0 \rightarrow {}^7F_1)$ was calculated as discussed above. Similarly, for $^5D_0 \rightarrow {}^7F_3$ and $^7F_5$ ED transitions, $k = 3$ and 5 ($\Omega_3 = \Omega_5 = 0$), so corresponding S_{ED} are also zero.

That is the reason why we're able to calculate only the luminescence branching ratios for transitions with J' = 1 ($\beta_{01} = 0.092$), J' = 2 ($\beta_{02} = 0.550$), J' = 4 ($\beta_{04} = 0.352$) and J' = 6 ($\beta_{06} = 0.006$).

6. Up-conversion luminescence

Emission spectrum for up-conversion luminescence (UCL) of studied glass under near-IR excitation at ~0.96 μm is presented in Fig. 4(a). The spectrum contains emission bands associated with transitions from metastable $^5D_0$ state of Eu^{3+} ions to lower-lying ^7F_J ones (J = 0, 1, 2, 3 and 4). Spectral position and relative intensity of these bands correspond to intrinsic emissions of Eu^{3+} under UV excitation.

Table 3
Emission lines of Eu^{3+} ions in Eu,Yb-doped oxyfluoride glass.

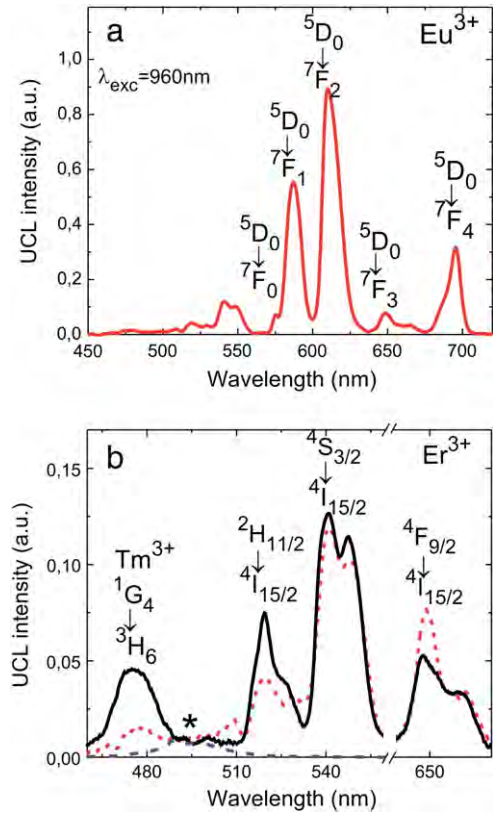| Transition	$^5D_1 \rightarrow$	$^5D_0 \rightarrow$				
	$^7F_2$	$^7F_0$	$^7F_1$	$^7F_2$	$^7F_3$	$^7F_4$
ν, cm^{-1}	18,348	17,301	16,920	16,340	15,337	14,285
λ, nm	545	578	591	612	652	700

Fig. 4. Up-conversion luminescence (UCL) of Eu,Yb-codoped oxyfluoride glass with the assignment of Eu^{3+} bands (a), Er^{3+} and Tm^{3+} impurity emissions of Eu,Yb-codoped glass (*red dashed* curve) and Yb-doped glass (*black solid* curve) with their assignment (b): excitation wavelength is 960 nm, * denote Yb^{3+} cooperative emission (*blue dash-dot* curve is the convolution of Yb^{3+} IR emission spectrum).

The scheme of this up-conversion process is presented in Fig. 5. As the energy of $^2F_{7/2}$ excited state of Yb^{3+} ions is near two times lower than that of metastable $^5D_0$ state, the direct energy transfer $Yb^{3+} \rightarrow Eu^{3+}$ cannot occur. However, in ytterbium-doped glasses two close Yb^{3+} ions can form a pair with "virtual" excited state. The energy of this state will be $2E(^2F_{7/2})$ that corresponds to the energy of $^5D_1$ state of Eu^{3+}. Thus, *cooperative* energy transfer (ET) from excited Yb^{3+} ion pair to single Eu^{3+} ion is possible. As a result, multicolor emissions of Eu^{3+} are possible. Fig. 5 also presents the mechanism of UV excitation of Eu^{3+} ions.

In order to confirm described mechanism of UCL, the dependence of emission intensity vs. excitation power was measured for most intense
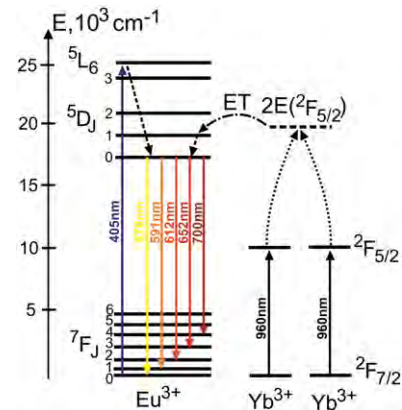

Fig. 5. Scheme of energy levels of Eu^{3+} and Yb^{3+} ions with marked excitation channels and radiative transitions from $^5D_0$ state.
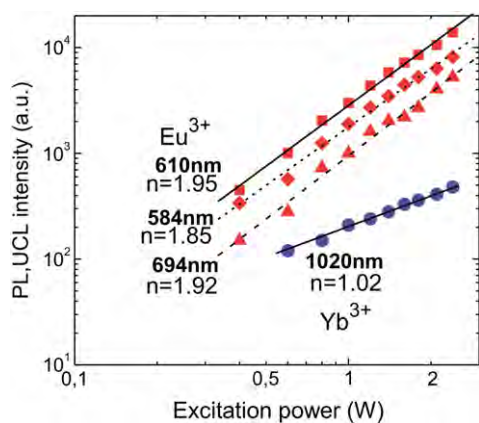
Fig. 6. log–log plots for UCL intensity vs. excitation power at 960 nm (n is the slope of dependencies); intrinsic emission of Yb^{3+} is analyzed for comparison (not in scale).

lines. For this, cw 3 W power-scalable InGaAs laser diode was used. The log–log plots of these dependencies are presented in Fig. 6. It also contains points measured at 1020 nm (intrinsic emission of Yb^{3+}, not in scale). Here points are experimental data, lines are their approximation. The slope of measured dependencies, n, indicates the number of excitation photons that take part in the UCL process. For the wavelengths of 591, 612 and 700 nm, $n = 1.85, 1.95$ and 1.92 ± 0.05. This clearly indicates two-photon nature of observed emissions. In contrast, $n = 1.02$ at 1020 nm, showing one-photon excitation channel for near-IR Yb^{3+} luminescence.

The *Commission internationale de l'éclairage* (CIE 1931) coordinates for synthesized glass phosphor are $x = 0.636$ and $y = 0.363$ that falls into the reddish-orange region. The CIE coordinates are calculated on the basis of measured UCL spectrum. For this, the spectral sensitivity of the luminescence set-up was accurately determined with halogen lamp with calibrated spectral power density. The monochomator was calibrated with Pb and Xe lamps. The dominant wavelength in the UCL spectrum is 604 nm with 98% purity. This agrees with value obtained for nanopowders, glasses and glass-ceramics doped solely with Eu^{3+}. Table 4 summarizes photoluminescent properties of studied glass.

7. Luminescence decay

For time-resolved luminescence studies, optical parametric oscillator tuned to 534 (excitation of Eu^{3+} to $^5D_1$ state) or 960 nm (excitation of Yb^{3+} to $^2F_{5/2}$ state) was used, pulse duration was 20 ns. The decay curve was detected with monochromator (SBW = 1 nm), fast

Hamamatsu C5460 photodetector (40 ns response time) and 500 MHz digital oscilloscope.

Fig. 7 shows luminescence decay curve for red Eu^{3+} emission at 612 nm. It is clearly single-exponential; the characteristic lifetime is $\tau_{exp} = 1550$ μs. The radiative lifetime of $^5D_0$ state calculated by modified J–O theory is $\tau_{rad} = 1595$ μs, indicating luminescence quantum yield ($\gamma = \tau_{exp} / \tau_{rad}$) approaching unity. This is consistent with large energy gap between $^5D_0$ state and lower-lying ^5F_J ones, as well as low phonon energies for oxyfluoride glasses.

Fig. 7 also shows decay curve for Yb^{3+} emission at 1020 nm (for two glasses, namely first one doped only with 1 mol% of YbF_3 and second one codoped with the same content of YbF_3, as well as 1 mol% of Eu_2O_3). The lifetimes of Yb^{3+} ions were measured for fine powdered samples immersed in glycerin in order to avoid the impact of reabsorption. The measured lifetimes for these two glasses are 980 (τ_D) and 880 (τ_{D-A}) μs. This shortening is attributed to $2Yb^{3+} \rightarrow Eu^{3+}$ ET, so we can estimate the efficiency of this process as $\eta_{ET} = 1 - (\tau_{D-A} / \tau_D) = 10 \pm 1\%$. The probability of energy transfer is then $p_{ET} = (1 / \tau_{D-A}) - (1 / \tau_D) = 120 \pm 10 \text{ s}^{-1}$. The observed decay curves are single-exponential.

An important comment is the role of competitive mechanism of shortening of lifetime of Yb^{3+} excited states. For our case, it can be (i) parasitic ET to impurity rare-earth ions like Er, Tm or Ho originating from YbF_3 or Yb_2O_3 reagents and (ii) cooperative luminescence of Yb^{3+}–Yb^{3+} pairs. The impact of both these effects can be easily estimated from UCL spectrum, Fig. 4(b). In this figure, the details of impurity emissions from both Yb, Eu-codoped and single Yb-doped glasses (with the same Yb content, glass composition, synthesis conditions, excitation power etc.) are presented.

For studied glass, weak traces of Er are detected. Indeed, emission bands around ~0.52, 0.54 and 0.65 μm correspond to UCL in the Yb^{3+}–Er^{3+} system due to transitions from $^2H_{11/2}$, $^4S_{3/2}$ and $^4F_{9/2}$ exited states to $^4I_{15/2}$ ground one. However, their integrated intensity is less than 2% from one of the Eu^{3+} emissions. UCL of Yb^{3+} ion pairs correspond to the spectral range of 0.48–0.51 μm, see blue dash-dot curve in Fig. 4(b) representing the convolution of IR emission spectrum of Yb^{3+} ions. For studied glass, this effect is near-vanishing. Thus, the main mechanism of the shortening of Yb^{3+} excited state lifetime is indeed $2Yb^{3+} \rightarrow Eu^{3+}$ ET. This is consistent with rather long $\tau_{exp}(Yb)$ that is close to ms values for best ytterbium laser glasses.

Particularly the aim of suppression of parasitic emissions motivates us to introduce Eu into the studied glass in the form of oxide, and Yb in the form of fluoride. In the preliminary experiment, we found that the same glass doped with Yb_2O_3 suffers from much stronger emissions of Er^{3+} and Tm^{3+} impurities, as well as cooperative Yb^{3+} luminescence. Indeed, previously it was shown that the doping precursor form can play a role in the cooperative effects in glasses [34].

8. Conclusions

Novel oxyfluoride glasses doped with 1 mol% of YbF_3 and Eu_2O_3 are synthesized in the SiO_2–PbO–PbF_2–CdF_2 system by melt-quenching technique. Their basic physical properties, as well as optical absorption and luminescence of Eu^{3+} and Yb^{3+} ions are studied. Spectroscopic properties of Eu^{3+} are modeled with modified Judd–Ofelt theory (SCI approximation), yielding absorption oscillator strength, luminescence branching ratios and radiative lifetime of $^5D_0$ state. Intrinsic emission of Eu^{3+} ions under direct excitation in the UV, as well as upconversion luminescence under near-IR excitation via cooperative ET, $2Yb^{3+} \rightarrow Eu^{3+}$, are studied. In the latter case, the glass provides intense reddish-orange emission with CIE coordinates $x = 0.636$, $y = 0.363$. The efficiency of observed ET mechanism is estimated from the shortening of $^2F_{5/2}(Yb^{3+})$ lifetime to be $10 \pm 1\%$. The glass has good potential for the production of up-conversion transparent glass-ceramics containing Eu,Yb:(Pb, Cd)F_2 nanocrystals with an even enhanced ET efficiency due to the precipitation of pure fluoride nanophase with good

Table 4
Summary of photoluminescent properties of Eu,Yb-doped oxyfluoride glass.

| Property	Value
λ_{exc}/transition	960 nm/$^2F_{7/2} \rightarrow ^2F_{5/2}$
Emission peak/transition	612 nm/$^5D_0 \rightarrow ^7F_2$
Luminescence branching ratios ($^5D_0 \rightarrow ^7F_J$)	0.092 ($J = 1$)
	0.550 ($J = 2$)
	0.352 ($J = 4$)
Asymmetry parameter R	8
Lifetime of $^5D_0$ state	1550 μs (measured)
	1595 μs (radiative)
CIE coordinates	$x = 0.636, y = 0.363$
Color	Reddish-orange
Dominant wavelength/purity	604 nm/98%
Efficiency of energy transfer, $2Yb^{3+} \rightarrow Eu^{3+}$	$10 \pm 1\%$
Judd–Ofelt parameters	$\Omega_2 = 9.6, \Omega_4 = 16.5,$ $\Omega_6 = 3.1 \, [10^{-20} \text{ cm}^2]$
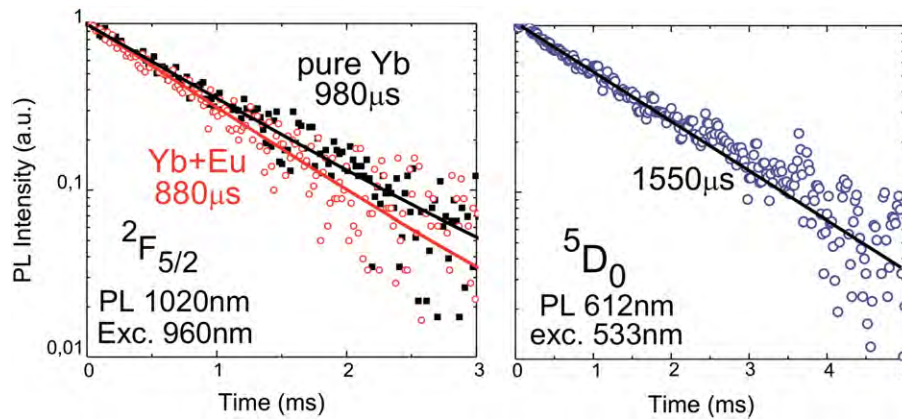
Fig. 7. Decay of near-IR Yb^{3+} luminescence for glass doped only with Yb and for glass codoped with Yb, Eu (*left* graph); decay of red Eu^{3+} luminescence (*right* graph).

spectroscopic properties, surrounded by amorphous oxide residual glass phase with proper thermal and mechanical ones.

References

[1] Y. Wang, J. Ohwaki, Appl. Phys. Lett. 63 (1993) 3268–3270.
[2] M. Takahashi, M. Izuki, R. Kanno, Y. Kawamoto, J. Appl. Phys. 83 (1998) 3920–3922.
[3] F. Auzel, D. Pecile, D. Morin, J. Electrochem. Soc. 122 (1975) 101–107.
[4] F.C. Guinhos, P.C. Nóbrega, P.A. Santa-Cruz, J. Alloys Compd. 323–324 (2001) 358–361.
[5] L. Feng, J. Wang, Q. Tang, L. Liang, H. Liang, Q. Su, J. Lumin. 124 (2007) 187–194.
[6] S. Ye, B. Zhu, J. Luo, J. Chen, G. Lakshminarayana, J. Qiu, Opt. Express 16 (2008) 8989–8994.
[7] M.D. Shinn, W.A. Sibley, M.G. Drexhage, R.N. Brown, Phys. Rev. B 27 (1983) 6635–6648.
[8] Y. Kishi, S. Tanabe, J. Alloy Compd. 408 (2006) 842–844.
[9] Z. Duan, J. Zhang, W. Xiang, H. Sun, L. Hu, Mater. Lett. 61 (2007) 2200–2203.
[10] M. Dejneka, E. Snitzer, R.E. Riman, J. Lumin. 65 (1995) 227–245.
[11] M.J. Dejneka, MRS Bull. 23 (1998) 57–62.
[12] Y. Kawamoto, R. Kanno, J. Qiu, J. Mater. Sci. 33 (1998) 63–67.
[13] F. Liu, E. Ma, D. Chen, Y. Yu, Y. Wang, J. Phys. Chem. B 110 (2006) 20843–20846.
[14] S. Tanabe, H. Hayashi, T. Hanada, N. Onodera, Opt. Mater. 19 (2002) 343–349.
[15] D. Chen, Y. Wang, Y. Yu, P. Huang, J. Phys. Chem. C 112 (2008) 18943–18947.
[16] G. Wakefield, E. Holland, P.J. Dobson, J.L. Hutchison, Adv. Mater. 13 (2001) 1557–1560.
[17] S.L. Jones, D. Kumar, R.K. Singh, P.H. Holloway, Appl. Phys. Lett. 71 (1997) 404–406.
[18] Y. Dwivedi, S.N. Thakur, S.B. Rai, Appl. Phys. B 89 (2007) 45–51.
[19] Y. Dwivedi, A. Rai, S.B. Rai, J. Lumin. 129 (2009) 629–633.
[20] G.S. Maciel, A. Biswas, P.N. Prasad, Opt. Commun. 178 (2000) 65–69.
[21] H. Wang, C. Duan, P.A. Tanner, J. Phys. Chem. C 112 (2008) 16651–16654.
[22] V. Jubera, A. Garcia, J.P. Chaminade, F. Guillen, J. Sablayrolles, C. Fouassier, J. Lumin. 124 (2007) 10–14.
[23] R. Martin-Rodriguez, R. Valiente, S. Polizzi, M. Bettinelli, A. Speghini, F. Piccinelli, J. Phys. Chem. C 113 (2009) 12195–12200.
[24] W. Strek, P.J. Deren, A. Bednarkiewicz, Y. Kalisky, P. Boulanger, J. Alloys Compd. 300–301 (2000) 180–183.
[25] Y. Dwivedi, D.K. Rai, S.B. Rai, Opt. Mater. 32 (2010) 913–919.
[26] X. Wei, J. Zhao, W. Zhang, Y. Li, M. Yin, J. Rare Earth 28 (2010) 166–170.
[27] B.R. Judd, Phys. Rev. 127 (1962) 750–761.
[28] G.S. Ofelt, J. Chem. Phys. 37 (1962) 511–519.
[29] E.B. Dunina, A.A. Kornienko, L.A. Fomicheva, Cent. Eur. J. Phys. 6 (2008) 407–414.
[30] A.A. Kornienko, A.A. Kaminskii, E.B. Dunina, Phys. Status Solidi B 157 (1990) 261–266.
[31] A.A. Kornienko, E.B. Dunina, V.L. Yankevich, Opt. Spectrosc. 81 (1996) 871–874.
[32] P.A. Loiko, V.I. Dashkevich, S.N. Bagaev, V.A. Orlovich, A.S. Yasukevich, K.V. Yumashev, N.V. Kuleshov, E.B. Dunina, A.A. Kornienko, S.M. Vatnik, A.A. Pavlyuk, J. Lumin. 153 (2014) 221–226.
[33] A.F. Kirby, F.S. Richardson, J. Phys. Chem. 87 (1983) 2544–2556.
[34] F. Auzel, P. Goldner, Opt. Mater. 16 (2001) 93–103.